Excited States and Photochemistry of Bicyclo[1.1.0]butane

Angelo R. Rossi*

Department of Chemistry The City University of New York - York College Jamaica, New York 11451

Yigui Wang and Kenneth B. Wiberg

Department of Chemistry Yale University New Haven, Connecticut 06520-8197

Received: August 18, 2008; Revised Manuscript Received: December 5, 2008

Calculations on the excited states of bicyclo[1.1.0]butane in the gas phase by different theoretical methods using several basis sets were performed. In general, the agreement between calculated and experimental excitation energies for bicyclo[1.1.0]butane in the gas phase is very good. Reviews of the solution-phase photochemistry of bicyclo[1.1.0]butane as well as previous calculations on the ground and excited states of bicyclo[1.1.0]butane are given to provide a necessary perspective of the photochemistry of bicyclo[1.1.0]butane in solution. To simulate the solution-phase photochemistry of bicyclo[1.1.0]butane, a well potential is added to the Kirkwood−Onsager model for obtaining solvation energies of molecules in solution. The addition of the well potential gives rise to a blue-shift of all gas-phase excitation energies in solution. However, there is also the very important added effect of providing an increase in Rydberg-valence mixing of solution-phase excited states. It is this mixing of antibonding valence character into the solution-phase excited states that is necessary to explain the solution-phase photochemistry of bicyclo[1.1.0]butane through bond-breaking and the formation of a conical intersection intermediate.

1. Introduction

The vacuum ultraviolet (VUV) spectrum of bicyclo[1.1.0]butane (**BCB**) has been examined in some detail,[1] and it is clear that the excited states are best described as Rydberg states with an electron in a diffuse orbital associated with a radical cation core.[2] The photochemistry of **BCB** has also been studied with irradiation of **BCB** at 185 nm in solution leading to both butadiene (**BD**) and **BCB**.[3] There has been an early MCSCF study of the electronically excited states of **BCB**.[4,5] The basic problem concerns how Rydberg states transform into valence states to yield the observed products. Recent developments have led to an ability to accurately determine the excited states of organic molecules. In this work, we examine the excited states of **BCB** with a view toward understanding which excited states lead to photochemical products.

2. Experimental Photochemistry of Bicyclo[1.1.0]butane

Berson et al.[3a] examined the photolysis of deuterium labeled **BCB**, which gave the following results:

SCHEME 1

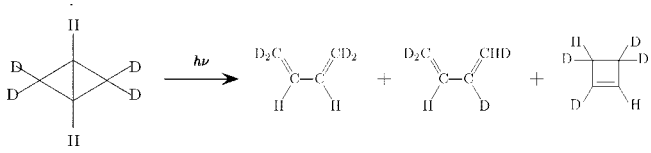

In this study, **BD**-*d4* was formed to a greater extent (10:1) than cyclobutene (**CB**). Another study indicated that the two products were formed in an approximately 1:1 ratio.[3b] To obtain further data, the photolysis of bicyclo[1.1.0]butane-2-^{13}C also was examined and suggested that there are two pathways for the photochemical reaction of **BCB**:

SCHEME 2

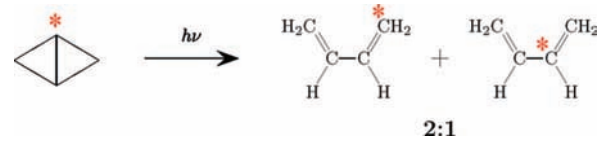

2:1

one that involves cleavage of the central C−C bond; and another in which the bridgehead bond is retained but diagonally opposite C−C bonds are broken to form the **BD** product. In view of the greater formation of **CB** in the later study, it is tempting to think that this product is initially formed from the cleavage of the C−C central bond and that **BD** is, in considerable measure, formed by its further photolysis, as shown by the possible following pathway:

SCHEME 3

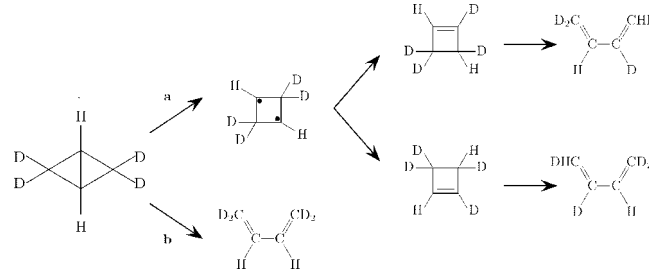

Butadiene-1,1,4,4-*d4* could also be formed by a concerted pathway for a symmetry-allowed disrotatory conversion of **BCB** to **BD** that retains the central C−C bond. However, the

* To whom correspondence should be addressed.

10.1021/jp807407c CCC: $40.75
Published on Web 02/03/2009

experimental results confirm a 2:1 ratio favoring pathway (a) over (b) for forming **BD**-*d4*.

3. Previous Calculations on Bicyclo[1.1.0]butane

3.1. Ground State. The thermal decomposition of **BCB** to **BD** has been studied in detail both experimentally[6] and theoretically.[7] The experimental studies and early CNDO study indicate that the thermal ring opening might pass through a symmetrical transition state (TS) by breaking two opposite side bonds at the same time and by rotating the two terminal CH_2 groups in a concerted symmetry-allowed conrotatory sense. This conclusion is in good accord with the Woodward−Hoffmann rules.[8] Using semiempirical MINDO/3 calculations, Dewar and Kirschner[7b] proposed a nonconcerted mechanism involving a diradical intermediate. Turro[9] showed that 1,8-naphthotricyclo-[4.1.0.0^{2,7}]heptane was converted to pleiadiene upon direct irradiation of light (<300 nm) but could also interconvert photochemically to the starting product, albeit by different mechanisms.

Performing MP2/3-21G calculations, Shevlin and McKee[7c] also suggested that the ring opening of **BCB** to form **BD** involves an asynchronous pathway with one C−C side bond substantially lengthened to produce a diradical. Nguyen and Gordon[7d] used accurate MCSCF calculations to obtain an activation barrier of ∼41 kcal mol^{-1} for a concerted, asynchronous, conrotatory, ring-opening of **BCB**, which leads directly to **BD**. In agreement with symmetry rules, they found that the disrotatory opening passed through a higher-energy transition state (∼67 kcal mol^{-1}).

Davis et al.[10] studied the isomerization of 1,3-tricyclo-[3.1.0.0^{2,6}]hexane using MCQDPT2 and CCSD(T) calculations at multiconfigurational and single-configurational levels of theory. They found that the isomerization process proceeded through an initial (*E*,*Z*)-1,3-tricyclo[3.1.0.0^{2,6}]hexadiene intermediate following a concerted, asynchronous pathway resulting from the conrotatory opening of the **BCB** fragment at a cost of ∼43 kcal mol^{-1}, which then travels over a small second barrier to the final (*Z*,*Z*)-1,3-tricyclo[3.1.0.0^{2,6}]hexadiene product. A second concerted pathway leading directly to (*Z*,*Z*)-1,3-tricyclo[3.1.0.0^{2,6}]hexadiene was also calculated to have an activation barrier of 54 kcal mol^{-1}.

The conrotatory and disrotatory mechanisms for the conversion of **BCB** to **BD** was again tested in a completely renormalized coupled-cluster (CR-CCSD(T) and CR-CC(2,3)) study by Kinal and Peicuch.[7e] Their results correctly predict the barrier for the conrotatory pathway, corresponding to a weakly biradical transition state with an activation barrier of 40.8 kcal mol^{-1} or ∼41.1 kcal mol^{-1}, in excellent agreement with experiment. The CR-CCSD(T) and CR-CC(2,3) methods also predict the correct barrier for the higher energy disrotatory pathway at ∼66−69 kcal mol^{-1}.

3.2. Excited States. The studies presented in the previous section establish the existence of a concerted, asynchronous pathway leading to an unsymmetrical transition state but complicate the idea of expecting simple symmetry rules that might control either thermal or excited-state reaction.

As discussed previously in section 2, experimental results for the photochemistry of **BCB**[3] indicate that the ring-opening might be the result of competing mechanisms. Srinivasan[11] showed that there was a connection between **BCB** and **BD** in the excited-state when a 5% solution of 1,3-butadiene in cyclohexane was photolyzed at 254 nm. Hopf et al.[12] demonstrated that direct irradiation of a dilute solution of 2,3-di-*tert*-butylbuta-1,3-diene in pentane using a 450 W Hg high-pressure lamp leads to the production of 1,2-di-*tert*-butylbicyclo[1.1.0]-butane. In contrast, the photolysis of the parent compound, buta-1,3-diene yields cyclobut-1-ene as the major product, and **BCB** is formed only in traces.[11]

Both detailed experimental spectral results and CIS studies showed that all low-lying excited states had mainly Rydberg character.[1,2] Early MCSCF studies[5] pointed qualitatively to competing mechanisms associated with different lower excited states based on electron populations, which excited states with strong C−C bridgehead bonds and others with strong C−C side bonds. Valence ionization potentials, low-lying electronically excited states, and other properties of **BCB**, tricyclopentane, tricyclohexane, and octabisvalene were investigated by Galasso[13] using Green's function techniques, the random phase approximation (RPA), and the equations-of-motions (EOM) approach. Reasonable values for ionization potentials and excited states were obtained when compared to compounds whose experimental results were known.

Computational evidence for a concerted formation of highly alkylated dienes to produce substituted **BCB** was provided by Garavelli et al.[14] The potential energy surfaces for the reaction of 1,3-butadiene to **CB** and **BCB** in the ground and lowest excited states were calculated by Sakai[15] using the CASSCF method. Rydberg functions were not included in the basis. The difference between the **CB** and **BCB** pathways is attributed to a dynamical momentum, which favors the **CB** pathway. A CASPT2//CASSCF study of mechanism for the photolysis of 2,3-diazobicyclo[2.1.1]hex-2-ene under direct irradiation[16] shows that, for the S_1 state, one C−N bond is broken first to generate a diazenyl radical, which then results in the **BCB** photochemical product through a concerted second C−N cleavage and C−C coupling process. A hybrid molecular mechanics/valence bond method to perform nonadiabatic dynamics calculations was used by Garavelli et al.[17] to explore the complex mechanism of the photolysis of s-cis butadiene, which undergoes several competing photochemical rearrangements. They found that both the experimental and simulated product distributions are in qualitative agreement.

4. Computational Details

Both ground- and excited-state calculations on **BCB** were performed using *Gaussian*,[18] *Gamess*,[19] *Molpro*,[20] and *MOLCAS*[21] programs. The EOM-CCSD excited states were calculated using *ACES II*.[22] The CASSCF calculations were carried out with the *Gaussian*,[18] *Gamess*,[19] *Molpro*,[20] and *MOLCAS*[21] programs. A 6-31G* basis[23] augmented with Rydberg s, p, and d functions was used as the basis set. The basis for the Rydberg functions was obtained from an STO-6G expansion using exponents 0.483 (3SP) and 0.333 (3D) derived from Slater's rules. The Rydberg functions were either added to the two-bridgehead carbon atom or placed at the center of geometry of **BCB**. The starting point of the active space for **BCB** is taken from Nguyen and Gordon[7d] (CASSCF(10,10)), which included five doubly bonded C−C framework molecular orbitals and their corresponding antibonding partners. To this reference space was added the diffuse s, p, and d Rydberg functions leading to

$$\underbrace{\mathrm{CASSCF(10,14)}}_{\substack{\mathrm{s+p}\\ \text{Rydberg Functions}}} \text{ and } \underbrace{\mathrm{CASSCF(10,20)}}_{\substack{\mathrm{s+p+d}\\ \text{Rydberg Functions}}}$$

active spaces. To include dynamical correlation energies, CASPT2[24] calculations were performed with the same basis set and active space.

Solvent effects were calculated using both the Kirkwood−Onsager[25] and polarizable continuum[26] models. To mimic the solute−solvent exchange repulsion, a repulsive well potential is added to the Kirkwood−Onsager model using the *MOLCAS* program.[27] The solvent used was cyclohexane. An important parameter in this model is the cavity size. A CASSCF calculation on the ground-state of **BCB** was performed with *Gaussian 03* using the volume keyword, which gave a value of the cavity radius $a = 3.52$ Å. Using the formula $a^3 = (3)/(4\pi N)V_m$, where V_m is the molar volume of cyclohexane and N is Avogadro's number, leads to the value $a = 3.50$ Å. The radial part of a Slater orbital can be expressed as

$$R(r) = r^{n-1}e^{-[(Z-S)/n^*]r} \quad (1)$$

where Z is the atomic number of the atom, S is the screening constant, n^* is the effective principal quantum number, and r is expressed in atomic units.

The mean value of the orbital radius, of an electron in a Slater orbital, shown in eq 1, is given by,[28]

$$\langle r^2\rangle = \left[\frac{n^*}{2(Z-S)}\right]^2(2n^2+1)(2n^*+2)a_0^2 \quad (2)$$

which yields $\langle r^2\rangle_{3s,3p} = 16.8$ Å^2 and $\langle r^2\rangle_{3d} = 35.3$ Å^2. Approximate values for the radial extent are then given as $r^{rms}_{3s,3p} \sim 4.1$ Å and $r^{rms}_{3d} \sim 5.9$ Å. If the cavity size is approximately 3.52 Å as determined above, then a significant portion of the electron density will penetrate into the solvent region.

Any attempt to optimize the cavity without the exchange repulsion term leads to the collapse of the solvent cavity. Because the SCRF model as implemented in *MOLCAS* allows for an additional exchange repulsion term between the solute and solvent, a minimum in energy can usually be obtained at a specific cavity radius. For the **BCB**−cyclohexane system, it was not possible to locate an energy minimum for the solvent cavity by optimizing the cavity radius with the Kirkwood−Onsager model plus the well potential. Instead, the effect of different cavity sizes on excitation energies was explored by assigning the center of the cavity, the origin of the well potential, and the **BCB** molecule at the origin of the coordinate system.

The SCRF model as proposed in *MOLCAS* is essential for understanding Rydberg states in solution. For excited valence states, the cavity size that is derived for the ground-state probably works within the PCM formalism, but for excited Rydberg states, where the spatial extent is extremely large, one has to include the repulsion term, otherwise there is leakage of the electron density into the dielectric continuum.

Studies of calculating gas-phase electronically excited states have demonstrated the importance of taking into account dynamical correlation. The SCRF model is incorporated into CASPT2 calculations by modifying the one-electron Hamiltonian yielding the CASPT2-RF approximation.

5. Experimental and Calculated VUV Spectra

5.1. Single-Determinant Methods. As part of our study, the results were obtained using single reference configuration methods including **CIS**,[29] **RPA**,[30] **TDDFT**,[31−33] and **EOM-CCSD**[30] methods. The ground-state structure was optimized at the MP2/6-31G* level and gives good agreement with the experimental structure.[2] The results for the first 10 excited states calculated at this geometry for several methods using the 6-311(2 + 2+)G** basis set are summarized in Table 1. Both the TD-B3P86 and the EOM-CCSD methods give good agreement with the experimentally observed excitation energies.[1,1b,34]

TABLE 1: Calculated Transition Energies in Electron Volts (eV) of BCB for Several Single-Determinant Methods Using the 6-311(2 + 2+)G Basis Set; the Oscillator Strengths[a] for Each Transition are Given in Parentheses**

state	CIS	RPA	TD-B3P86	EOM-CCSD	observed
$2A_1$	6.80(0.001)	6.79(0.001)	6.20(0.000)	6.27(0.000)	6.1
$3A_1$	7.17(0.046)	7.16(0.043)	6.53(0.044)	6.61(0.042)	6.6
$1B_2$	7.38(0.000)	7.38(0.000)	6.65(0.000)	6.80(0.000)	
$1B_1$	7.19(0.041)	7.18(0.039)	6.64(0.023)	6.70(0.032)	6.6
$2B_2$	8.10(0.007)	8.09(0.008)	7.46(0.007)	7.65(0.005)	
$4A_1$	8.11(0.001)	8.10(0.001)	7.29(0.000)	7.59(0.000)	
$2B_2$	8.13(0.011)	8.13(0.010)	7.35(0.009)	7.63(0.011)	
$1A_2$	8.14(0.000)	8.13(0.000)	7.49(0.000)	7.68(0.000)	
$5A_1$	8.17(0.002)	8.16(0.002)	7.35(0.001)	7.70(0.002)	
$6A_1$	8.35(0.000)	8.35(0.000)	7.52(0.001)	7.93(0.000)	

[a] Oscillator strength: $f = (^2/_3)(m_e)/(\hbar^2)(E_2 - E_1)\sum_i^N\sum_{\alpha=x,y,z}|\langle\Psi_1|r_{i,\alpha}|\Psi_2\rangle|^2$.

5.2. CASSCF and CASPT2 Results. The CASSCF and CASPT2 results for **BCB** are summarized in Table 2.

The experimental and simulated spectra at EOM-CCSD and TD-B3P86 levels are shown in Figure 1, whereas similar spectra derived from TDDFT methods can be found in Figure 2. The simulated VUV spectra are obtained by representing each excited-state peak by an analytical Lorentzian function, and the whole spectrum is the sum of contributions from all of these peaks on a point-by-point basis. The bump in the TD-B3P86 simulated spectrum in Figure 1 is due to the cutoff of a tail for a strong peak at high energy.

Whereas both the EOM-CCSD and TD-B3P86 methods agree fairly well with the experimental spectrum as shown in Figure 1, it can be seen from Figure 2 that the BLYP and B3LYP functionals underestimate the experimental excitation energies. On the other hand, the B3P86 functional yields excellent agreement with the experimental spectrum but the M052X functional shifts the spectrum to higher energy.

6. Adiabatic Excited States

6.1. Excitation Energies and Geometries. The adiabatic excited states of **BCB** may be important in its photochemistry. The excited-state energies for both neutral **BCB** and its radical cation using the CIS/6-311(2+,+)G**, TD-B3LYP/6-311++G**, and EOM-CCSD/6-311++G** methods are presented in this section. The CIS/6-311(2+,+)G** method is related to Hartree−Fock and does not include correlation effects, the TD-B3LYP/6-311++G** method is related to TDDFT and includes some of the effects of electron correlation, whereas the EOM-CCSD/6-311++G** method is generally considered to be one of the most satisfactory single determinant methods for including electron correlation. Because the core region of Rydberg states is similar to that of **BCB** radical cation, one would expect the geometry of adiabatic excited states to adopt structure similar to the radical cation core. In Table 3, the optimized structures and vertical and excitation energies at the CIS/6-311(2+,+)G** level are given for first few adiabatic excited states. This expectation is confirmed except for the 1^1B_1 state, which has a much longer central bond length than that of radical cation (∼2.0 Å vs ∼1.7 Å). The radical cation itself has longer central bond than the ground state (∼1.7 Å vs ∼1.5 Å).

Basis sets are a concern in our calculations for vertical excited states, as discussed previously in section 5. To further investigate the effect of basis sets, excited states of **BCB** were optimized using a 6-31G(d,p) basis + diffuse Rydberg functions on the bridgehead carbons. These calculations yielded structures similar

TABLE 2: CASSCF and CASPT2 Results of BCB

state	configuration	CASSCF[a,b]	CASPT2[a,b]	experiment[b]	oscillator strength[c]	$\langle r^2 \rangle$ [d]
1^1A_1	$\cdots(7a_1)^2$	−155.006493	−155.391221			
						15.6
2^1A_1	$\cdots(7a_1)^1(3s)^1$	−154.791466	−155.164322	∼6.1		
		5.85	6.17		0.001	30.5
1^1B_1	$\cdots(7a_1)^1(3p_x)^1$	−154.788285	−155.149284	∼6.6		
		5.94	6.58		0.052	30.2
1^1B_2	$\cdots(7a_1)^1(3p_y)^1$	−154.779542	−155.145588			
		6.18	6.76		0.000	31.8
1^1A_2	$\cdots(7a_1)^1(3d_{xy})^1$	−154.757695	−155.117543			
		6.77	7.45		0.256	47.8
1^2A_1	$\cdots(7a_1)^1$	−154.717103	−155.064290	∼9.1		
		7.87	8.89		0.000	11.3

[a] Total energies are in atomic units (au). [b] Excitation energies are in electron volts (eV). [c] Oscillator strength: $f = f = (^2/_3)(m_e)/(\hbar^2)(E_2 - E_1)\sum_i^N \sum_{\alpha=x,y,z}|\langle\Psi_1|r_{i,\alpha}|\Psi_2\rangle|^2$. [d] $\langle r^2 \rangle$ are in units of Å^2.

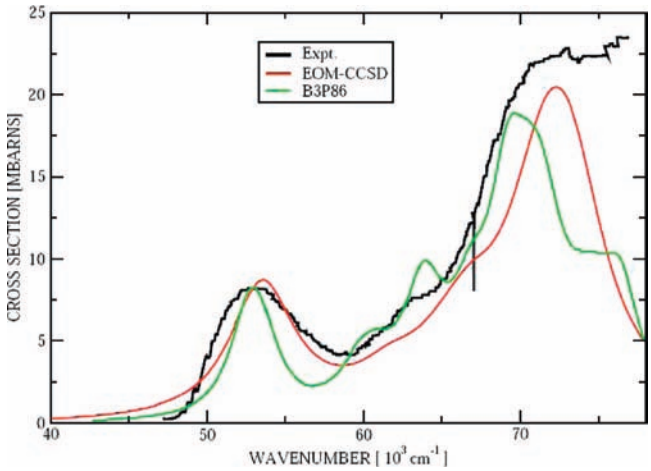

Figure 1. Experimental and simulated VUV spectra at the EOM-CCSD and TD-B3P86 levels of approximation using the 6-311(2 + 2+)G** basis set.

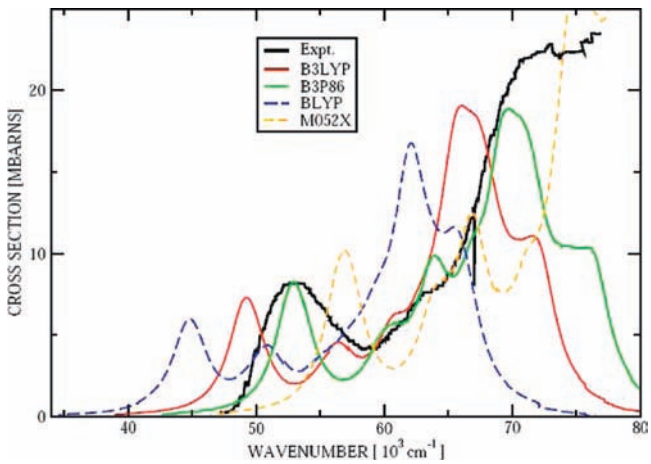

Figure 2. Simulated spectra of BCB using representative TD-DFT methods with the 6-311(2 + 2+)G** basis set.

to those listed in Table 3. The calculated C−H bridgehead bond distance averaged over all states is 1.085 Å. For the CH_2 group in **BCB**, the two C−H bond lengths averaged over all of the states are 1.091 and 1.103 Å. The smaller basis sets for the adiabatic 1^1B_1 excited state shows that the diffuse function in 6-31+G* reduces the vertical excitation energy by ∼2.4 eV, yet has only minor effects on the optimized structure of the adiabatic excited-state and the adiabatic excitation energy. The adiabatic excited-state structures at the CIS/6-31+G* level generally confirm the findings at the CIS/6-311(2+,+)G** level.

TABLE 3: Excited-State Properties of BCB Calculated with C_{2v} Symmetry Employing the CIS/6-311(2+,+)G Method[a]**

	Energies (eV)[b]		Structural Parameters[c] (Å)		
state	vertical	adiabatic	bridgehead C−C	side bond C−C	puckering angle[d] $CH_2-\bullet-CH_2$
1^1A_1	0.00	0.00	1.503	1.503	121.8
2^1A_1	6.80	6.00(5.36)	1.709	1.480	135.7
1^1B_1	7.19	5.42(1.97)	1.976	1.484	156.6
1^1B_2	7.38	6.55(5.84)	1.722	1.484	134.8
2^1B_1	8.10	6.83(5.49)	1.797	1.490	142.5
1^2A_1		7.37	1.699	1.492	133.8

[a] Structures for the ground- and excited-neutral states, as well as radical cation structures, of **BCB** are calculated at the HF/6-311-(2+,+)G** level. [b] Values in parentheses are optimized structures at the CIS/6-311(2+,+)G** level. [c] For the CH_2 group in **BCB**, the two C−H bond lengths averaged over all states are 1.084 and 1.100 Å. [d] $CH_2-\bullet-CH_2$ is defined as the puckering angle in degrees where • is the midpoint of the C−C bridgehead bond.

Correlation effects are also important for obtaining accurate adiabatic excited-state structures. The CIS method is based on Hartree−Fock, so correlation effects are not included. Results at TD-B3LYP/6-311++G** level for 13 lower excited states provide results similar to those for CIS/6-31+G*. However, the optimization of the 1^1B_1 excited-state was not successful because the excitation energy becomes very small (<1 eV) when the central bond is stretched to ∼2.0 Å, and convergence problems arose presumably because many additional configurations were required.

In the family of single reference methods, EOM-CCSD includes the correlation effects through the coupled cluster theory and is a reliable method for the study of excited states. The results for the EOM-CCSD/6-311++G** method are listed in Table 4. An extremely long central bond in the 1^1B_1 excited-state is again found. It is interesting that the first excited 1^1B_2 state has a *shorter* central bond than the ground state.

The results of optimized excited states for **BCB** calculated with single-determinant reference wave functions including CIS, RPA, TDDFT with several exchange potentials and EOM-CCSD are obtained in the gas phase and cannot be directly compared with those CASSCF and CASPT2 results that include solvent effects for excited states and photochemical pathways. However, they do provide an adequate description of the excited-state spectrum as well as important structural parameters.

7. Solute−Solvent Exchange Repulsion in Solution

Cramer[35] provides an excellent discussion of implicit solvation models in helping to understand the physical nature of con-

TABLE 4: Excited-State Properties of BCB Calculated with C_{2v} Symmetry Employing the EOM-CCSD/6-311++G Method[a]**

State	Energies (eV)[b]		Structural Parameters[c] (Å)		
	verticle	adiabatic	bridgehead C−C	side bond C−C	puckering angle[d] CH_2-•-CH_2
1^1A_1	0.00	0.00	1.501	1.501	121.8
2^1A_1	6.49	5.55(5.41)	1.671	1.488	135.4
1^1B_1	6.98	5.34(3.16)	1.934	1.481	152.8
1^1A_2	7.07	6.17(6.01)	1.681	1.495	133.2
1^1B_2	8.30	7.44(7.07)	1.387	1.576	106.4
1^2A_1		8.54	1.695	1.496	133.8

[a] Structures for the ground- and excited-neutral states, as well as radical cation structures, of **BCB** are calculated at the EOM-CCSD/6-311(+,+)G** level. [b] Values in parentheses are optimized structures at the CIS/6-311(2+,+)G** level. [c] The calculated C−H bridgehead bond distance averaged over all states is 1.076 Å. [d] CH_2−•−CH_2 is defined as the puckering angle in degrees where • is the midpoint of the C−C bridgehead bond.

densed systems. In this section, we will expand on this discussion to specifically take into account the exchange repulsion between the solute and solvent, which is purely a quantum mechanical effect.

For the polarizable continuum model (PCM),[26] the free energy of solvation (ΔG_{sol}) is typically partitioned into electrostatic (ΔG_{elect}) and nonelectrostatic ($\Delta G_{nonelect}$) terms. The electrostatic component is calculated by an ab initio treatment for a solvent in a polarizable continuum, neglecting solute−solvent coupling interactions related to dispersion and exchange repulsion. The nonelectrostatic terms, including cavitation, dispersion, and repulsion, are computed directly using classical expressions involving pair potentials and empirical expressions related to the surface area of atoms. There have been recent attempts[36,37] to simultaneously evaluate the electrostatic solute charge distribution, exchange repulsion, and dispersion contributions in a self-consistent manner upon solvation. Results were obtained for four solvents including water, octanol, chloroform, and carbon tetrachloride using both Hartree−Fock (HF) and DFT for a wide variety of basis sets which pointed to a solvent-dependence of dispersion and repulsion terms. Whereas the quality of the basis set had little effect of the repulsion component, it did influence the dispersion component. Particularly for water, the agreement between the quantum mechanical-SCRF and classical treatments of dispersion and repulsion was reasonably good. The quantum mechanical-SCRF[36,37] methods were developed at the HF and DFT levels and did not include dynamic correlation. In addition, the results were calculated only for ground-state properties.

The basic idea behind the effective fragment potential (EFP) model[38−40] as applied to a solute−solvent system is to replace the solvent molecules with rigid fragments, which can interact with the solute molecule through nonbonded interactions. The solute molecule is represented by an ab initio wave function, whereas the nonbonded interactions implemented in the EFP include coulomb interactions, dipole polarizabilities, and repulsive potentials both between EFPs and between the EFP and the ab initio system.

Another approach by Karlström[41] involves studying the solute molecule by quantum mechanical methods and the surrounding solvent as two components: part dielectric continuum and part discrete solvent representation. The explicit representation component allows for the effect of both dispersion and Pauli exchange repulsion.

TABLE 5: Parameters Used in the Self-Consistent Reaction Field Model for Cyclohexane

dielectric constant, ϵ		2.023	
cavity radius[a], a		10.0	
length of multipole expansion, l_{max}		4	
Pauli repulsion parameters, V_{PR}	w_i	β_i	$r_{0,i}$[a]
	1.0	5.0	12.0
	1.0	3.5	13.0
	1.0	2.0	15.0
	1.0	1.4	17.0

[a] Values are in atomic units.

For the Kirkwood−Onsager model,[25] the surrounding solvent molecules are approximated by a dielectric continuum. A spherical cavity, with radius a, is surrounded by a dielectric continuum,

$$H = H_\circ + H_{RF} + H_{WP} \tag{3}$$

and the generalized cavity field is given as

$$\Phi_l^m = \frac{1}{4\pi\epsilon_\circ}\frac{(l+1)(\epsilon-1)}{(l+1)\epsilon+1}\frac{\mu_l^m}{a^{2l+1}} \tag{4}$$

The energy contribution from the induced field is computed from the interaction between the multiple moments of the solute molecule and the electric field induced by them:

$$E_{RF} = -\frac{1}{2}\sum_{l,m}\Phi_l^m\mu_l^m \tag{5}$$

This is a crude approximation because only electrostatic effects are taken into account while dispersion and repulsive effects are ignored.

Bernhardsson et al.[42] and Serrano[43] augmented the cavity model with an approximation to describe the Pauli repulsion of the solvent electrons and the molecular solute, which forces the solute electrons to remain in the cavity and not penetrate the surrounding surrounding dielectric continuum. The Pauli exchange repulsion is modeled by a potential (V_{PR}) to describe the solute−solvent interaction. A repulsive well potential is added to the Kirkwood−Onsager model to avoid leakage of charge outside the cavity:

$$V_{PR} = \int\int\int \rho(r,\theta,\phi)f(r)\,dr\,d\phi\,d\theta \tag{6}$$

and

$$f(r) = \sum_i w_i e^{-\beta_i(r-r_{0,i})^2} \tag{7}$$

where w_i is a weighting factor, β_i an exponent, and $r_{0,i}$ is the radius of each spherical shell function. The parameters used for the self-consistent reaction model for cyclohexane are given in Table 5.

7.1. Excited States of BCB in Solution. When a molecule, like **BCB**, is excited to a Rydberg state in the gas phase, the excited electron can freely expand to the available volume. The same Rydberg excited-state in solution will have a severely constrained spatial extent and experience a strong electronic repulsion with the surrounding solvent molecules. These effects must be taken into account in any model that describes the excited states and subsequent photochemistry of **BCB**.

Performing CASSCF-SCRF and CASPT2-RF calculations with a repulsive potential[42] on formamide and *N*-methylacetamide, Besley and Hirst[44] showed that the Rydberg states are destabilized by the Pauli repulsion with the solvent. Crespo et al.[45] found that the lowest two excited Rydberg states in

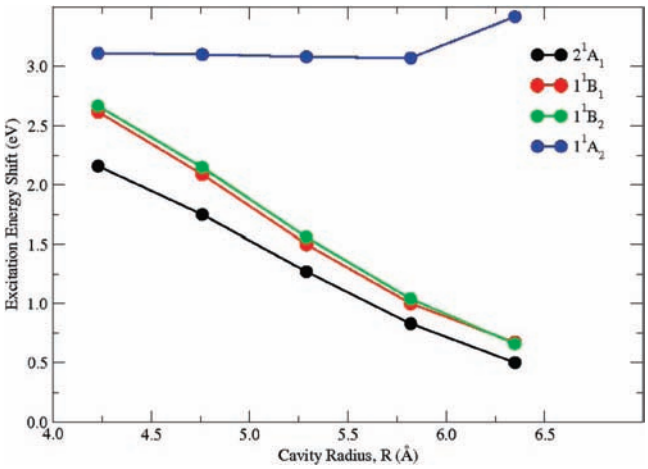

Figure 3. CASPT2 shifts of excitation energies for BCB in solution relative to the gas phase using cyclohexane solvent as a function of cavity radius, a and employing an extended Kirkwood−Onsager model which includes a V_{PR} term.

n-tetrasilane are selectively blue-shifted when it is embedded in a rare gas cluster.

7.2. Properties of Excited States of BCB in Solution. Our calculations mimic the effect of solvent−solute repulsion by observing the trend in properties of excited states, and the cavity radius is varied as shown in Figure 3.

The shifts in excitation energies shown in Figure 3 provide useful insight into the influence of cyclohexane solvent on the electronic spectrum of **BCB**. As the cavity radius decreases, the shift in excitation energy *increases* for the low-lying 2^1A_1, $^1B_1$, $^1B_2$ and excited states because these states are *below* the excited valence manifold, and the solvent destabilizes these diffuse Rydberg states through the Pauli repulsion. The 2^1A_1 state shows the lowest shift in excitation energy, in comparison to the $^1B_1$ and $^1B_2$ states, because it has a large dipole moment leading to an increased reaction-field stabilization as discussed below. On the other hand, the shift in excitation energy for the $^1A_2$ initially *decreases* and then remains constant at most cavity sizes for $a < 6$Å. The $^1A_2$ excited-state lies *above* the excited valence manifoled and is extremely diffuse but becomes essentially valence in character at smaller cavity sizes. All excited Rydberg states converge to their valence excited-state partners as the cavity shrinks. The compact nature of valence states makes them less susceptible to repulsive interactions. As the cavity radius is increased to ∼6.5 Å, the $^1A_2$ becomes Rydberg and shows an increased shift in excitation energy. As the cavity size increases even more, the effect of the repulsive potential becomes negligible, the Rydberg states of **BCB** begin to stabilize, and the excitation energies approach the gas-phase values, yielding smaller shifts. For a larger cavity radius, the Pauli repulsion is sufficiently weak, the Rydberg states are no longer heavily penalized, and the Rydberg transitions approach the gas-phase values.

Results obtained for excited Rydberg states in the gas phase and in cyclohexane solution are given in the Table 6. The extended Kirkwood−Onsager model with a V_{PR} term between the solvent and solute yields a larger blue shift for all excited states rather than the standard Kirkwood−Onsager model. The repulsive V_{PR} term shifts the $^1A_2$ state above the ionization limit and has clearly been converted into a valence state. Note, that the expectation values of $\langle r^2 \rangle$ are reduced for the excited states of **BCB** when a V_{PR} term is introduced. This reduction in $\langle r^2 \rangle$ reflects a shrinkage of the excited-state orbitals brought about by an increase in valence mixing together with a concomitant

TABLE 6: Transition Energies[a], Radial Extent[b], and Dipole Moment[c] (μ) for BCB in the Gas Phase and Cyclohexane Solvent[d] Using the Kirkwood−Onsager Model Both With and Without a Repulsive Potential

	Gas Phase			Cyclohexane Solvent					
state	ΔE^{Ex}	$\langle r^2 \rangle$	μ	$\Delta E^{Ex}_{V_{PR}}$	$\langle r^2 \rangle$	μ	ΔE^{Ex}	$\langle r^2 \rangle$	μ
$^1A_1$	0.00	15.6	0.8721	0.00	16.7	0.7922	0.00	15.8	0.8186
2^1A_1	6.30	30.5	8.2811	7.44	26.5	8.1649	6.37	30.4	7.3628
$^1B_1$	6.69	30.2	0.0724	8.08	27.3	0.3637	6.73	29.4	2.2196
$^1B_2$	6.77	31.8	2.6678	8.32	27.8	0.1598	6.90	31.5	1.3790
$^1A_2$	7.45	47.8	0.8063	10.54	16.3	1.0413	7.42	47.8	0.8320
$^2A_1$	8.79	11.3	0.7815	9.03	11.3	0.7884	8.99	11.3	0.8096

[a] Transition energies were calculated using CASPT2. [b] $\langle r^2 \rangle$ is in units of Å^2. [c] μ is in units of Debye. [d] Calculations with cyclohexane solvent employed a cavity radius, a = 5.29 Å for the extended Kirkwood−Onsager model with a V_{PR} term and a = 3.52 Å for the standard Kirkwood−Onsager model.

reduction in Rydberg orbital character. The net effect is that the influence of a repulsive potential provides a constraining force on the outer excited electrons to a smaller region of space. This orbital constraint allows Rydberg-valence mixing and changes the nature of excited states for BCB in solution. From this result, the photochemistry from excited states of **BCB** is expected to be influenced by the solvent. In contrast, the spatial extent, $\langle r^2 \rangle$, for the standard Kirkwood−Onsager model is the same as for the gas phase. This model exhibits little difference between the excited states of **BCB** in the gas phase or in solvent and represents an inadequate representation of excited Rydberg states in solution.

The Born energy for a dipole in its reaction field is given by

$$G_{\text{dipole}} = -\frac{1}{2}\mu E_{\text{reaction field}} = \frac{\mu^2}{4\pi\epsilon_0 a^3}\left(\frac{\epsilon_0 - \epsilon}{2\epsilon - \epsilon_0}\right) \qquad (8)$$

where μ is the dipole moment, $E_{\text{reaction field}}$, the reaction field, a, the cavity radius, and ϵ_0 and ϵ are the dielectric constants of the solute and solvent, respectively. Using eq 8, one can see that the reaction field energy is directly related to the magnitude of the dipole moment. This result is reflected in Table 6 where the 2^1A_1 excited-state has a very large dipole moment and yields a stabilization energy that is larger than for the other excited states and in Figure 3 where the shift in excitation energy is smallest.

The repulsive potential was not parametrized for organic solute/organic solvent interactions and, consequently, the interaction between **BCB** and cyclohexane imparted by the repulsive well potential (V_{PR}) is, perhaps, too large, leading to very strong repulsive interactions. But the important point is that a repulsive potential is needed to reflect an essential component for cavity models that deal with the interaction of a solute surrounded by a dielectric continuum.

7.3. Rydberg Populations for Excited States of BCB In Solution. Rydberg populations for excited states of **BCB** in the gas phase and in cyclohexane solution are given in Table 7. Whereas the dependence of the Mulliken overlap population on basis sets is well-known[46] and should be used with caution when diffuse basis functions are present, it is possible to look at trends in populations with a fixed basis set. The Rydberg populations for the gas phase and standard Kirkwood−Onsager potential are essentially identical, which is very similar to the trend for $\langle r^2 \rangle$ seen in Table 6. Thus, there is very little effect on the composition of Rydberg states in the absence of a model including Pauli repulsion. On the other hand, when the Pauli repulsion is included via a well potential, there is a significant

TABLE 7: Comparison of Rydberg Populations for BCB Ground and Excited States in the Gas Phase and Solution

		Rydberg Population		
			solution[a]	
state	configuration	gas phase	no well	well
1^1A_1	$\cdots (7a_1)^2$	0.04	0.04	0.04
2^1A_1	$\cdots (7a_1)^1(3s)^1$	1.01	1.02	0.79
1^1B_1	$\cdots (7a_1)^1(3p_x)^1$	1.03	1.03	0.88
1^1B_2	$\cdots (7a_1)^1(3p_y)^1$	1.06	1.06	0.87
1^1A_2	$\cdots (7a_1)^1(3d_{xy})^1$	1.02	1.02	0.05

[a] The solution calculations were obtained for cyclohexane solvent employing a cavity radius, $a = 5.29$ Å for the extended Kirkwood−Onsager model with a V_{PR} term (well), and $a = 3.52$ Å for the standard Kirkwood−Onsager model (no well).

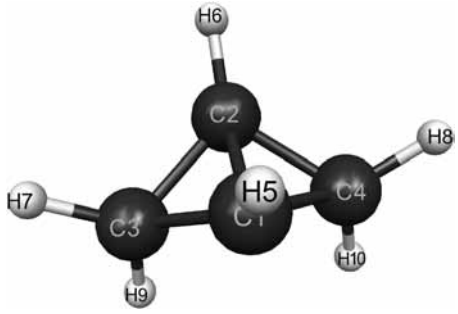

Figure 4. Figure of **BCB** along with atom numbering.

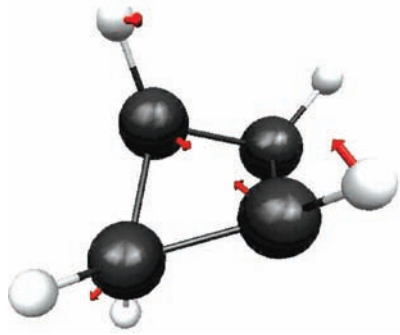

Figure 5. Lowest vibrational mode for the 2^1A_1 excited state of **BCB** in the gas phase having a normal-mode frequency of 703.13 cm^{-1}.

drop in Rydberg population and reflects a mixing of valence character into the excited states. This Rydberg-valence mixing leads to important consequences for the photochemistry of **BCB** as will be discussed in section 8. Whereas the theoretical underpinnings of including a well potential term to mimic Pauli repulsion may not be rigorous, the trend in results clearly demonstrates that it is needed to induce valence-Rydberg mixing, which, in turn, impacts the photochemistry by incorporating an important valence contribution.

8. Photochemical Pathways of BCB

8.1. Excited States and Solution Photochemistry. Although **BCB**, shown in Figure 4, and **BD** are structural isomers, they are different in many aspects, and it is interesting to make a comparison between them.

BCB is relatively rigid, whereas **BD** is quite flexible. **BD** has trans and gauche isomers with the trans isomer approximately 3.0 kcal mol^{-1} lower in energy than the gauche. **BD** has a conjugated π system resulting in strong absorption peaks around 6.0 eV in VUV spectra.[47] In contrast, the lack of a π system in **BCB** results in weak absorptions starting at ~6.7 eV.[1] The reactivity of **BD** has been favorite subject for validating the Woodward−Hoffmann rules[8] and also the subject of detailed studies of conical intersections.[48,49] As discussed in section 3.2, calculations on the pathway for the photochemical transformation of **BCB** to **BD**[14,15] have been performed previously.

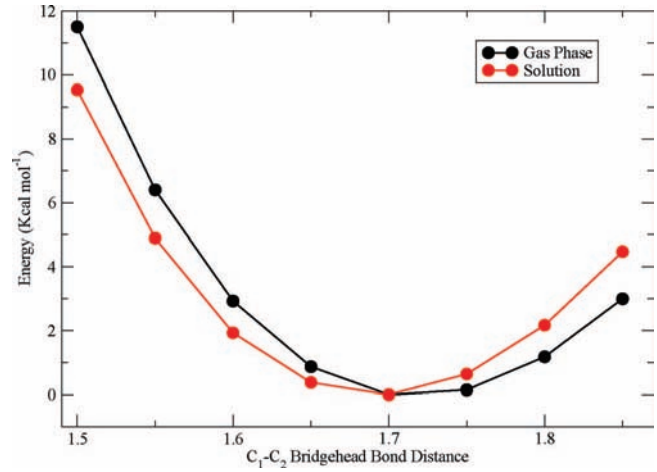

Figure 6. Stretching/compressing energy as a function of the C_1-C_2 bond distance for the 2^1A_1 excited state of **BCB** both in the gas phase and solvent calculated with the CASSCF method.

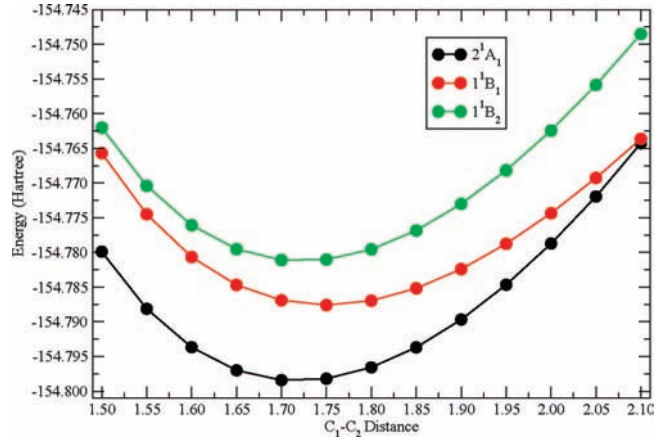

Figure 7. Relaxed potential-energy curves for low-lying excited states in the gas phase obtained from CASSCF calculations.

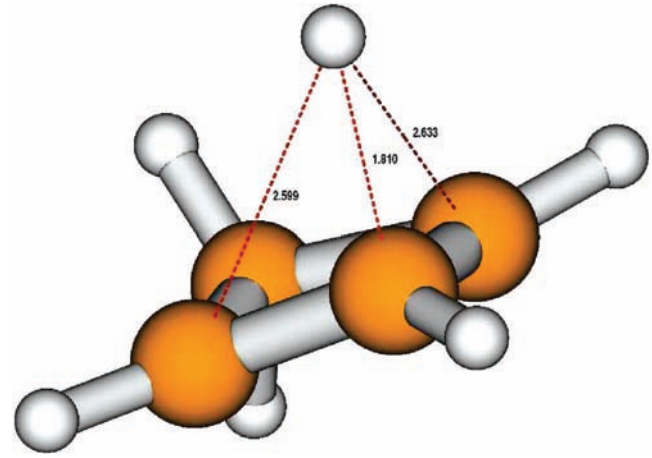

Figure 8. CASSCF(10,11)/6-31G*(Ry) optimized conical intersection intermediate derived from mixing the ground 1^1A_1 state of **BCB** and the excited-state 2^1A_1 dimethylenecyclobutane diradical, resulting in methylene C−H bond cleavage and hydrogen migration To a region hovering above three carbon atoms.

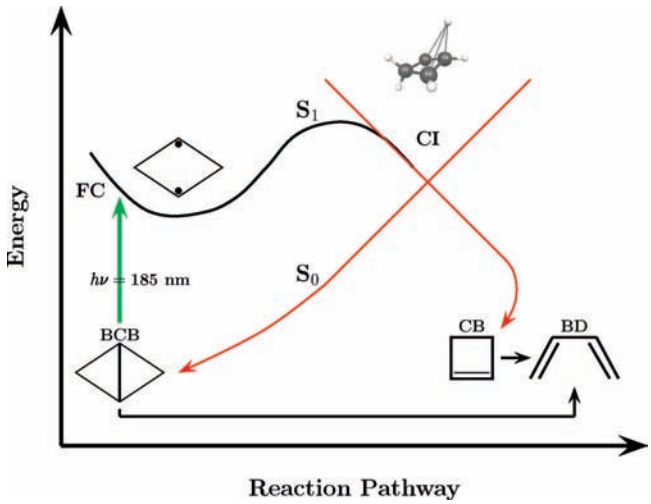

Figure 9. Schematic diagram for the Franck−Condon (FC) excitation of **BCB** to the 2^1A_1 state, which relaxes to a diradical intermediate. This is then followed by the formation of a conical intersection intermediate (CI) by a nonadiabatic pathway. The CI produces cyclobutene (**CB**) or reverts to **BCB**. Vibrationally excited **BCB** can produce butadiene (**BD**) directly.

In this section, we present both a unifying thread for the photochemical decomposition of **BCB** into its products, which include both **BD** and **CB** and the influence of solvent on the photochemical pathway and product distribution. There are three essential features of the solution-phase photochemistry, which may account for the products:

1. The increased composition of valence antibonding orbital character for excited states of **BCB** in solution, as shown by Table 7, can promote bond breaking.

2. There is a cage effect in solution, which imposes constraints on the formation resulting from photochemistry.

For example, the qualitative dimensions of **BCB** are 3.3 Å × 2.8 Å × 4.8 Å versus 5.5 Å × 3.0 Å for **BD**. Thus, the larger size of **BD** may give rise to increased solvent repulsion along the pathway for ring opening, allowing other pathways for the formation of products such as **CB** (2.6 Å × 2.7 Å × 1.7 Å) to become more competitive.

The cage effect may also be operative in the bond opening and closing of the C_1-C_2 bond formed initially from excited states of **BCB**.

That the cage effect may be operative can be seen from a vibrational analysis performed on the minimum energy structure of the 2^1A_1 excited state. It was found to be a true energy minimum having all real vibrational frequencies. The lowest vibrational normal mode involves the stretching/compression of the C_1-C_2 bond and is shown in Figure 5.

The low gas-phase normal-mode frequency of 703.13 cm^{-1} allows the C_1-C_2 bond to be easily stretch or compressed as is shown in Figure 6. Note that it is slightly easier to perform this motion in solution.

3. A key role in the photochemical mechanism for **BCB** is a nonadiabatic process, which passes through a conical intersection, leading directly to the **CB** photochemical product and a reversion to the **BCB** reactant via two ground-state reaction pathways.

A unique feature for all the low-lying excited states of **BCB**, both in the gas phase and in solution, involves the weakening bridge head C−C bond, as shown in Figures 6 and 7. As seen in Figure 6, the intermediate obtained from the 2^1A_1 excited-state has an equilibrium bond distance of 1.7 Å, but only ∼5−10 kcal mol^{-1} is required to compress the C_1-C_2 bond to ∼1.5 Å. This is important because, subsequent to excitation, the C_1-C_2 bond opens and closes many times allowing facile formation of a conical section by mixing of the ground 1^1A_1 and excited 2^1A_1 states.

8.2. Photochemical Products and Conical Intersections. The pathway for photochemical reactions generally proceeds from excited-state reactants to ground-state products. For pathways characterized as having a conical intersection (CI) associated with radiationless decay,[49] the photochemistry for the excited-state reactions of **BCB** will be very efficient.

The existence of a concerted photochemical pathway for [1,2] and [1,3] alkyl sigmatropic shifts was shown to go through a conical intersection by Bernardi et al.[50] Wilsey and Houk reported conical intersections for *hydrogen/vinyl* and *alkyl/vinyl* reactions.[51] A type of conical intersection intermediate, which contains a triangular arrangement of three carbon centers, corresponding to a $-(CH)_3-$ unit with a hydrogen atom hovering above, appears to be a general feature of conjugated systems.[49,52,53] At the CASSCF(10,11)/6-31G*(Ry) level, a CI intermediate, shown in Figure 8, was obtained and found to be 5.69 eV above the ground state. The CI falls nicely into this class of intermediates, and the energy above the ground state is well within the 185 nm VUV wavelength used in the experiments.

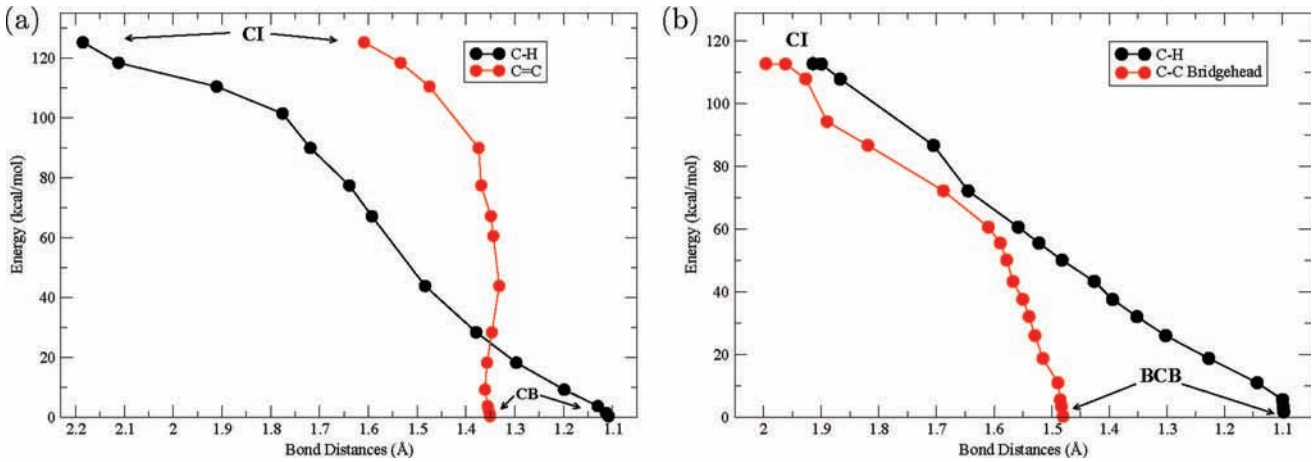

Figure 10. Minimum energy pathways for CI → cyclobutene (**CB**) formation (a) and CI → **BCB** reversion (b) obtained from CASPT2(6,6)/6-31G* calculations. (a) The reference energy is taken as the lowest value on each MEP surface. (b) The CASSCF(6,6) active space included three doubly occupied orbitals; two π allyl molecular orbitals, one bonded to the hydrogen atom, and their antibonding counterparts; and two C−C σ and σ^* molecular orbitals. To include dynamical correlation energies, CASPT2[24] calculations were also performed within this active space.

A schematic diagram showing excitation of **BCB** to the 2^1A_1 state followed by formation of a diradical resulting from scission of the C−C bridgehead bond and conversion to a CI section is shown in Figure 9. Subsequently, this CI is responsible for the formation of **CB** or reversion to potentially vibrationally hot **BCB**. Minimum energy pathways (MEP) in which the energy is plotted versus the C−H distance for the migrating hydrogen atom and the C−C distance for the reversion to **BCB** or formation of **CB** from the CI are shown in parts a and b of Figure 10, respectively. The change in C−H distances reflect movement of the hydrogen atom above three carbon atoms shown in Figure 8 to the CH_2 groups of either **CB** or **BCB**. The change in C−C distances indicate bridgehead formation in **BCB** or double-bond formation for **CB**. Note, that the MEP energetic pathways proceed directly downhill in both cases.

The hot ground-state **BCB** most likely results in a concerted, asynchronous, conrotatory, ring-opening to **BD** similar to the findings of Nguyen and Gordon.[7d] Thus, an efficient pathway to form both **BD** and **CB** products proceeds through a conical intersection.

The CI shown in Figure 8 also explains the **BD** product that has one CHD terminal group when 2,2,4,4-deuterium substituted **BCB** is irradiated with far-UV light. When reactant **BCB** is substituted with ^{13}C at the 2-position, the **BD** product may result with the ^{13}C at either middle or end positions. It is possible to devise a scheme where the intermediate from Figure 8 can be invoked to produce an intermediate diradical yielding **CB**, which subsequently converts to **BD** with ^{13}C substituted according to Schemes 1 and 2. But early studies of the isotope effect of hydrocarbons showed that substitution of ^{13}C for ^{12}C was small[54] and would have little effect on changing product ratios or accounting for the mechanism of ^{13}C substitution.

9. Conclusions

The calculations presented in this article provide a nonintuitive result for the far UV photochemistry of **BCB** in solution, especially the pathway for the formation of **BD** product. The gas-phase excitation energies for both single-deteminant **CIS**, **RPA**, **TDDFT**, and **EOM-CCSD** and **CASPT2** methods are in excellent agreement with the experimental values and are found to have Rydberg character. Because all of the excited states of **BCB** lead to an opening of the bridgehead bond, it is difficult for the side bonds to undergo a concerted disrotatory opening to produce **BD**. All attempts to find an excited-state adiabatic pathway for the conversion of **BCB** to **BD** in the gas phase proved unsuccessful.

Condensed-phase calculations are essential to understanding product formation of excited **BCB** because the effect of solution is to increase valence mixing of the ground and excited states with antibonding character to weaken bonds. This mixing also provides an enhanced ability to produce a CI intermediate where the following conditions are fulfilled: the energies of the two surfaces at the CI point are equal ($E_{2^1A_1} - E_{1^1A_1} = 0$); and the derivatives of difference in energy with respect to $q = 3, 4, \cdots, 3N - 8$ degrees of freedom (x_q) are equal to zero ($(\partial(E_{2^1A_1} - E_{1^1A_1}))/(\partial x_q) = 0$). Note that two independent variables (x_1 and x_2) are needed to define a conical intersection.

The most likely conclusion is that excitation to the 2^1A_1 state in solution is responsible for two competing reactions; on the one hand, the conical intersection intermediate produces a vibrationally hot **BCB** ground-state, which converts to **BD** in a manner similar to the thermal ground-state reaction (part b of Scheme 3); on the other hand, the formation of **CB** is produced directly from the conical section intermediate as a result of a [1,2]-H shift. However, the **BD** product could also be formed from further reaction though electrocyclic ring opening of **CB**. That this is a possibility might help explain the differences in product ratios obtained by Becknell et al.[3a] and Adam et al.[3b] because excessive irradiation may have been used in the former experiment, which yielded more **BD** as a secondary product by further irradiating the **CB** that is formed from the CI pathway.

Acknowledgment. One of the authors (A.R.R.) would like to thank Dr. R. Srinivasan for his helpful comments about the far UV phothochemistry of **BCB**. He would also like to thank the staff at the Arctic Regional Supercomputer Center (http://www.arsc.edu) who provided a generous grant of computer time and constant support for this project.

References and Notes

(1) (a) Wiberg, K. B.; Ellison, G. B.; Peters, K. S. *J. Am. Chem. Soc.* **1977**, *99*, 3941. (b) Wiberg, K. B.; Peters, K. S.; Ellison, G. B.; Alberti, F. *J. Am. Chem. Soc.* **1977**, *99*, 3946.

(2) Walters, V. A.; Hadad, C. M.; Thiel, Y.; Colson, S. D.; Wiberg, K. B.; Johnson, P. M.; Foresman, J. B. *J. Am. Chem. Soc.* **1991**, *113*, 4782–4791.

(3) (a) Becknell, A. F.; Berson, J. A.; Srinivasan, R. *J. Am. Chem. Soc.* **1985**, *107*, 1076–1078. (b) Adam, W.; Oppenländer, T.; Zhang, G. *J. Am. Chem. Soc.* **1985**, *107*, 3921–3924. (c) Adam, W.; Oppenländer, T. *Angew. Chem., Int. Eng. Ed.* **1986**, *25*, 661–672.

(4) Bent, G. D.; Rossi, A. R. *J. Phys. Chem.* **1991**, *95*, 7228–7223.

(5) Bent, G. D. *J. Phys. Chem.* **1992**, *96*, 8084–8089.

(6) (a) Chesick, J. P. *J. Phys. Chem.* **1964**, *68*, 2033–2034. (b) Wiberg, K. B.; Lavanish, J. M. *J. Am. Chem. Soc.* **1966**, *88*, 5272–5275. (c) Closs, G. L.; Pffer, P. E. *J. Am. Chem. Soc.* **1968**, *90*, 2452–2453. (d) Srinivasan, R.; Levi, A. A.; Haller, I. *J. Am. Chem. Soc.* **1965**, *65*, 1775–1777. (e) Frey, H. M.; Stevens, I. D. R. *Trans. Faraday Soc.* **1965**, *61*, 90–94.

(7) (a) Wiberg, K. B. *Tetrahedron* **1968**, *24*, 1083–1096. (b) Dewar, M. J. S.; Kirschner, S. *J. Am. Chem. Soc.* **1975**, *97*, 2931–2932. (c) Shevlin, P.; McKee, M. *J. Am. Chem. Soc.* **1988**, *110*, 1666–1671. (d) Nguyen, K. A.; Gordon, M. S. *J. Am. Chem. Soc.* **1995**, *117*, 3835–3847. (e) Kinal, A.; Piecuch, P. *J. Phys. Chem. A* **2007**, *111*, 734–742.

(8) Woodward, R. B.; Hoffmann, R. *The Conservation of Orbital Symmetry*; Verlag Chemie, Academic Press: New York, 1970.

(9) Turro, N. J.; Ramamurthy, V.; Pagni, R. M.; Butcher, J. A., Jr. *J. Org. Chem.* **1977**, *42*, 92–96.

(10) Davis, S. R.; Nguyen, K. A.; Lammertsma, K.; Mattern, D. L.; Walker, J. E. *J. Phys. Chem. A* **2003**, *107*, 198–203.

(11) Srinivasan, R. *J. Am. Chem. Soc.* **1963**, *85*, 4045–4046.

(12) Hopf, H.; Lipka, H.; Traettemberg, M. *Angew. Chem., Int. Eng. Ed.* **1994**, *33*, 204–205.

(13) Galasso, V. *Int. J. Quantum Chem.* **1996**, *57*, 587–594.

(14) Garavelli, M.; Frabboni, B.; Fato, M.; Celani, P.; Bernardi, F.; Robb, M. A.; Olivucci, M. *J. Am. Chem. Soc.* **1999**, *121*, 1537–1545.

(15) Sakai, S. *Chem. Phys. Lett.* **2000**, *319*, 687–694.

(16) Chen, H.; Li, S. *J. Org. Chem.* **2006**, *71*, 9013–9022.

(17) Garavelli, M.; Bernardi, F.; Olivucci, M.; Bearpark, M. J.; Klein, S.; Robb, M. A. *J. Phys. Chem. A* **2001**, *105*, 11496–11504.

(18) Frisch, M. J.; Trucks, G. W.; Schlegel, H. B.; Scuseria, G. E.; Robb, M. A.; Cheeseman, J. R. J. A. Montgomery, J.; Vreven, T.; Kudin, K. N.; Burant, J. C.; Millam, J. M.; Iyengar, S. S.; Tomasi, J.; Barone, V.; Mennucci, B.; Cossi, M.; Scalmani, G.; Rega, N.; Petersson, G. A.; Nakatsuji, H.; Hada, M.; Ehara, M.; Toyota, K.; Fukuda, R.; Hasegawa, J.; Ishida, M.; Nakajima, T.; Honda, Y.; Kitao, O.; Nakai, H.; Klene, M.; Li, X.; Knox, J. E.; Hratchian, H. P.; Cross, J. B.; Bakken, V.; Adamo, C.; Jaramillo, J.; Gomperts, R.; Stratmann, R. E.; Yazyev, O.; Austin, A. J.; Cammi, R.; Pomelli, C.; Ochterski, J. W.; Ayala, P. Y.; Morokuma, K.; Voth, G. A.; Salvador, P.; Dannenberg, J. J.; Zakrzewski, V. G.; Dapprich, S.; Daniels, A. D.; Strain, M. C.; Farkas, O.; Malick, D. K.; Rabuck, A. D.; Raghavachari, K.; Foresman, J. B.; Ortiz, J. V.; Cui, Q.; Baboul, A. G.; Clifford, S.; Cioslowski, J.; Stefanov, B. B.; Liu, G.; Liashenko, A.; Piskorz, P.; Komaromi, I.; Martin, R. L.; Fox, D. J.; Keith, T.; Al-Laham, M. A.; Peng, C. Y.; Nanayakkara, A.; Challacombe, M.; P. M. W. Gill Johnson, B.; Chen, W.; Wong, M. W.; Gonzalez, C.; Pople, J. A. *Gaussian 03, Revision C.02 and IBM64-G03, RevC.02 12-Jun-2004*, Gaussian, Inc., Wallingford CT, 2004.

(19) Schmidt, M. W.; Baldridge, K. K.; Boatz, J. A.; Elbert, S. T.; Gordon, M. S.; Jensen, J. H.; Koseki, S.; Matsunaga, N.; Nguyen, K. A.; Su, S. J.; Windus, T. L.; Dupuis, M.; Montgomery, J. A. *J. Comput. Chem.* **1993**, *14*, 1347–1363.

(20) Werner, H.-J.; Knowles, P. J.; Lindh, R.; Manby, F. R.; Schütz, M.; Celani, P.; Korona, T.; Rauhut, G.; Amos, R. D.; Bernhardsson, A.;

Berning, A.; Cooper, D. L.; Deegan, M. J. O.; Dobbyn, A. J.; Eckert, F.; Hampel, C.; Hetzer, G.; Lloyd, A. W.; McNicholas, S. J.; Meyer, W.; Mura, M. E.; Nicklass, A.; Palmieri, P.; Pitzer, R.; Schumann, U.; Stoll, H.; Stone, A. J.; Tarroni, R.; Thorsteinsson, T. *MOLPRO, version 2006.1, a package of ab initio programs*, 2006, see http://www.molpro.net.

(21) Karlström, G.; Lindh, R.; Malmqvist, P.; Roos, B. O.; Ryde, U.; Veryazov, V. P.-O.; Widmark, M. C.; Schimmelpfennig, B.; Neogrady, P.; Seijo, L. *Comput. Mater. Sci.* **2003**, *28*, 222–239.

(22) Stanton, J.; Gauss, J.; Watts, J.; Nooijen, M.; Oliphant, N.; Perera, S.; Szalay, P.; Lauderdale, W.; Kucharski, S.; Gwaltney, S.; Beck, S.; Balková, A.; Bernholdt, D.; Baeck, K.; Rozyczko, P.; Sekino, H.; Hober, C.; Bartlett, R. *ACES II is a program product of the Quantum Theory Project, University of Florida. Integral packages included are* **VMOL** (J. Almlöf and P. R. Taylor); **VPROPS** (P. R. Taylor); **ABACUS** (T. Helgaker, H. J. Aa. Jensen, P. Jørgensen, J. Olsen, and P. R. Taylor).

(23) (a) Hehre, W. J.; Ditchfield, R. J. A.; Pople, J. A. *J. Chem. Phys.* **1972**, *56*, 2257. (b) Harihan, P. C. J. A.; Pople, J. A. *Theor. Chim. Acta* **1973**, *28*, 213.

(24) (a) Werner, H. J. *Mol. Phys.* **1996**, *89*, 645. (b) Celani, P.; Werner, H. J. *J. Chem. Phys.* **2000**, *112*, 5546.

(25) (a) Kirkwood, J. G. *J. Chem. Phys.* **1939**, *7*, 911. (b) Onsager, L. *J. Am. Chem. Soc.* **1936**, *58*, 1486. (c) Tapia, O.; Goscinski, O. *Mol. Phys.* **1975**, *29*, 1653.

(26) Miertus, S.; Scrocco, E.; Tomasi, J. *J. Chem. Phys.* **1981**, *55*, 117.

(27) Serrano-Andrés, L.; Moriarity, N. *MOLCAS Version 7.0 User's Manual*, 2007. http://www.teokem.lu.se/molcas/, Tutorials and Examples, pp 271−481.

(28) Hirschfelder, J. O.; Wahl, A. C. In *Slater Screening Constants in Atomic and Molecular Orbitals*; Löwdin, P.-O., Ed.; Academic Press, New York, 1966; p 217.

(29) Foresman, J. B.; Head-Gordon, M.; Pople, J. A.; Frisch, M. J. *J. Phys. Chem.* **1992**, *96*, 2096–2135.

(30) Stanton, J. F.; Bartlett, R. J. *J. Chem. Phys.* **1993**, *98*, 7029–7039.

(31) Stratmann, R. E.; Scuseria, G. E.; Frisch, M. J. *J. Chem. Phys.* **1998**, *109*, 8218–8224.

(32) Bauernschmitt, R.; Ahlrichs, R. *Chem. Phys. Lett.* **1996**, *256*, 454–464.

(33) Casida, M. E.; Jamorski, C.; Casida, K. C.; Salahub, D. R. *J. Chem. Phys.* **1998**, *108*, 4439–4449.

(34) Robin, M. B. Saturated Absorbers. In *Higher Excited States of Polyatomic Molecules*; Academic Press: New York and London, 1974; Vol. I, pp 152, 155.

(35) Cramer, C. J. In *Essentials of Computational Chemistry. Theories and Models*, 2nd ed.; John Wiley & Sons. Ltd., 2004; Chapter 11, pp 385−427.

(36) Amovilli, C.; Mennucci, B. *J. Phys. Chem. B* **1997**, *101*, 1051–1057.

(37) Curutchet, C.; Orozco, M.; Luque, F.; Mennucci, B.; Tomasi, J. *J. Comput. Chem.* **2006**, *27*, 1769–1780.

(38) Day, P. N.; Jensen, J. H.; Gordon, M. S.; Webb, S. P.; Stevens, W. J.; Krauss, M.; Garner, D.; Basch, H.; Cohen, D. *J. Chem. Phys.* **1996**, *105*, 1968–1986.

(39) Chen, W.; Gordon, M. S. *J. Chem. Phys.* **1996**, *105*, 11081–11090.

(40) *GAMESS User's Guide, April 13*, 2008. http://www.msg.ameslab-.gov/GAMESS/, Section 4 - Further Information, The Effective Fragment Potential Method, pp 159−167.

(41) (a) Karlström, G. *J. Phys. Chem.* **1988**, *92*, 1318–1322. (b) Öhrn, A.; Karlström, G. *Mol. Phys.* **2006**, *104*, 3087–3099. (c) Öhrn, A.; Karlström, G. *J. Phys. Chem. A* **2006**, *110*, 1934–1942. (d) Tofteberg, T.; Öhrn, A.; Karlström, G. *Chem. Phys. Lett.* **2006**, *429*, 436–439. (e) Öhrn, A.; Karlström, G. *Theor. Chem. Acc.* **2007**, *117*, 441–449.

(42) Bernhardsson, A.; Lindh, R.; Karlström, G.; Roos, B. O. *Chem. Phys. Lett.* **1996**, *251*, 141–149.

(43) (a) Serrano-Andrés, L.; Fülshcer, M. P.; Karlström, G. *Int. J. Quantum Chem.* **1997**, *65*, 167–181. (b) Serrano-Andrés, L. *Solvent Effects in MOLCAS*; MOLCAS Workshop 2008: Training Workshop on Computational Quantum Chemistry in Bojnice, Slovakia, June 9−13, 2008.

(44) Besley, N. A.; Hirst, J. D. *J. Phys. Chem. A* **1998**, *102*, 10791–10797.

(45) Crespo, R.; Teramae, H.; Antic, D.; Michl, J. *Chem. Phys.* **1999**, *244*, 203–214.

(46) (a) Young, D. C. In *Population Analysis*; John Wiley & Sons: NewYork, 2001; Chapter 12, pp 99−105. (b) Bachrach, S. M. Population Analysis and Electron Densities from Quantum Mechanics. In *Reviews in Computational Chemistry*; Lipkowitz, K. B., Boyd, D. B., Eds.; VCH Publishers, Inc.: New York, 1994; Vol. 5, Chapter 3, pp 171−222.

(47) Wiberg, K. B.; Rosenberg, R. E. *J. Am. Chem. Soc.* **1990**, *112*, 1509–1519.

(48) Sicilia, F.; Blancafort, L.; Bearpark, M. J.; Robb, M. A. *J. Phys. Chem. A* **2007**, *111*, 2182–2192.

(49) Olivucci, M.http://ccmaol1.chim.unisi.it/comp-photochem, Computational Organic Photochemistry.

(50) Bernardi, F.; Olivucci, M.; Robb, M. A.; Tonachin, G. *J. Am. Chem. Soc.* **1992**, *114*, 5805–5812.

(51) (a) Wilsey, S.; Houk, K. N. *J. Am. Chem. Soc.* **2002**, *124*, 11182–11190. (b) Wilsey, S.; Houk, K. N. *Photochem. Photobiol.* **2002**, *76*, 616–621. (c) Wilsey, S.; Houk, K. N. *J. Am. Chem. Soc.* **2000**, *122*, 2651–2652. (d) Wilsey, S.; Houk, K. N.; Zewail, A. H. *J. Am. Chem. Soc.* **1999**, *121*, 5772–5786.

(52) Palmer, I. J.; Ragazos, I. N.; Bernardi, F.; Olivucci, M.; Robb, M. A. *J. Am. Chem. Soc.* **1993**, *115*, 673–682.

(53) Celani, P.; Garavelli, M.; Ottani, S.; Bernardi, F.; Robb, M. A.; Olivucci, M. *J. Am. Chem. Soc.* **1995**, *117*, 11584–11585.

(54) (a) Bigeleisen, J.; Wolfsberg, M. *J. Chem. Phys.* **1953**, *21*, 1972–1974. (b) Bigeleisen, J.; Wolfsberg, M. Theoretical and Experimental Aspects of Isotope Effects in Chemical Kinetics. In *Adv. Chem. Phys.* Interscience Publishers, Inc.: New York, 1958; Vol. 1, pp 15−76. (c) Bigeleisen, J. *J. Phys. Chem.* **1958**, *56*, 823–828.

JP807407C